Hearing Research 416 (2022) 108429

Contents lists available at ScienceDirect

Hearing Research

journal homepage: www.elsevier.com/locate/heares

Research Paper

Semi-automated quantification of hair cells in the mature mouse utricle

Cathy Yea Won Sung, Melanie Barzik, Tucker Costain, Lizhen Wang, Lisa L. Cunningham*

Laboratory of Hearing Biology and Therapeutics, National Institute on Deafness and Other Communication Disorders (NIDCD), NIH, Bethesda, Maryland, USA

ARTICLE INFO

Article history:
Received 24 June 2021
Revised 19 November 2021
Accepted 28 December 2021
Available online 14 January 2022

Keywords:
Hair cells
Utricle
Pou4f3
Activated caspase 3/7
Myosin 7a, ImageJ

ABSTRACT

The mouse utricle model system is the best-characterized *ex vivo* preparation for studies of mature mammalian hair cells (HCs). Despite the many advantages of this model system, efficient and reliable quantification of HCs from cultured utricles has been a persistent challenge with this model system. Utricular HCs are commonly quantified by counting immunolabeled HCs in regions of interest (ROIs) placed over an image of the utricle. Our data indicate that the accuracy of HC counts obtained using this method can be impacted by variability in HC density across different regions of the utricle. In addition, the commonly used HC marker myosin 7a results in a diffuse cytoplasmic stain that is not conducive to automated quantification and must be quantified manually, a labor-intensive task. Furthermore, myosin 7a immunoreactivity is retained in dead HCs, resulting in inaccurate quantification of live HCs using this marker. Here we have developed a method for semi-automated quantification of surviving HCs that combines immunoreactivity for the HC-specific transcription factor Pou4f3 with labeling of activated caspase 3/7 (AC3/7) to detect apoptotic HCs. The discrete nuclear Pou4f3 signal allowed us to utilize the binary or threshold function within ImageJ to automate HC quantification. To further streamline this process, we created an ImageJ macro that automates the process from raw image loading to a final quantified image that can be immediately evaluated for accuracy. Within this quantified image, the user can manually correct the quantification via an image overlay indicating the counted HC nuclei. Pou4f3-positive HCs that also express AC3/7 are subtracted to yield accurate counts of surviving HCs. Overall, we present a semi-automated method that is faster than manual HC quantification and identifies surviving HCs with high accuracy.

1. Introduction

Aminoglycoside antibiotics are widely used to treat life-threatening bacterial infections, and cisplatin is a platinum-based chemotherapy drug that is highly effective in treating a variety of cancers. However, both treatments have ototoxic side effects that lead to permanent loss of sensory hair cells (HCs) in the inner ear, resulting in permanent hearing loss and/or balance disorders. Cisplatin is the most ototoxic drug in clinical use, resulting in permanent hearing loss in up to 90% of patients (Coradini et al., 2007; Fausti et al., 1994; Marshak et al., 2014), while aminoglycoside treatment causes hearing loss in approximately 20% of treated adults (Huth et al., 2011; Petersen and Rogers, 2015). These high incidences of hearing loss emphasize the importance of developing therapies to prevent or reverse ototoxicity.

Whole-organ cultures of utricles from adult mice represent a well-characterized *ex vivo* preparation for studying the responses of mature mammalian HCs and supporting cells (SCs) to ototoxic drugs (Bucks et al., 2017; Burns et al., 2012a; Cunningham, 2006; Jen et al., 2019; Kaur et al., 2015; Sayyid et al., 2019). The mature mouse utricle contains approximately 3200–4000 HCs (Burns et al., 2012b; Desai et al., 2005; Golub et al., 2012). Thus, manually counting all utricular HCs is labor-intensive and time-consuming. To bypass these challenges, utricular HC survival is often quantified within preselected regions of interest (ROIs). Within these ROIs, myosin 7a-positive HCs are manually counted to calculate the average HC density (Baker et al., 2015; Breglio et al., 2020; Sayyid et al., 2019; Zhang et al., 2020). However, this method can inaccurately reflect the HC counts from the whole utricle due to the variability of HC density in different regions of the utricle. For instance, the

HCs, Hair cells; SCs, Supporting cells; AC3/7, Activated caspase 3/7; ROI, Region of Interest; ES, Extrastriola; P-ES, Posterior extrastriola; M-ES, Medial extrastriola; L-ES, Lateral extrastriola; SD, Standard deviation; NGS, Normal Goat Serum.

* Corresponding author.
E-mail address: lisa.cunningham@nih.gov (L.L. Cunningham).

https://doi.org/10.1016/j.heares.2021.108429

striolar region contains fewer HCs than the extrastriolar region (ES) and is considerably more susceptible to ototoxic drug treatment (Cunningham et al., 2004; Ono et al., 2020; Woodson, 2013). Here, we have explored how ROI placement across the utricle impacts the accuracy of HC counts. We observed differential susceptibility to ototoxic drug treatment across different ES regions of the utricle. Consequently, these regional differences result in inconsistent HC counts that depend on the placement of the ROIs on the utricle. We have eliminated the dependency on ROI placements by developing a method to semi-automatically quantify HCs in the entire utricle, thus, removing any regional bias. Our method uses Pou4f3, a well-characterized HC nuclear marker conducive to automated cell counting. This automated counting enables HC quantification from the entire utricle. In addition, our method uses co-labeling with activated caspase 3/7 (AC3/7) to distinguish living vs. dead HCs. To further automate HC quantification, we created a macro written in the ImageJ software package (NIH, Bethesda, MD) to streamline this process. Upon comparison with manual HC counts from four independent researchers, the semi-automated approach was significantly faster while reliably producing accurate and reproducible HC counts.

2. Methods

Animals. All animal procedures were approved by the combined ACUC of the National Institute on Deafness and Other Communication Disorders (NIDCD) and the National Institute of Neurological Disorders and Stroke (NINDS) (protocol no. 1327). 4–10-week old C57BL/6J (stock no. 000664) or CBA/J (stock no. 000656) mice were purchased from The Jackson Laboratory (Bar Harbor, ME, USA). HC-specific Gfi1$^{Cre/+}$ mice (generated by Lin Gan, University of Rochester, Rochester, NY, USA) were a kind gift from Ronna Hertzano (University of Maryland, College Park, MD, USA). Offspring of Gfi1$^{Cre/+}$ mice were crossed with a transgenic reporter mouse line B6.Cg-*Gt(ROSA)26Sortm14(CAG-tdTomato)Hze*/J (The Jackson Laboratory, stock no. 007914) to generate mice that express tdTomato in HCs (Gfi1-tdTomato). Quantification of tdTomato-positive HCs from this breeding scheme revealed >90% recombination efficiency in HCs from cultured utricles in addition to Cre recombination in resident macrophages of the inner ear as previously described (Matern et al., 2017; Sadler et al., 2020; Stone et al., 2018). In a pilot experiment, approx. 1% of cells in the sensory epithelium of control utricles were [tdTom+/Pou4f3-], suggesting they were tdTom+ cells that were not HCs; while approximately 0.4% of cells were [tdTom-/Pou4f3+], suggesting they were dead HCs (data not shown). Approximately equal numbers of male and female mice were used in each experiment. Mice were exposed to the standard alternating 12 h light /12 h dark cycle.

Utricle cultures. Mice were euthanized using CO_2 followed by decapitation. Utricles were dissected from both left and right inner ear and cultured as previously described (Brandon et al., 2012; Cunningham, 2006). Briefly, the bony labyrinth of the mouse inner ear was removed and placed in Medium 199 (Gibco, Thermo Fisher Scientific, cat# 12350–039). Utricles were further dissected from the bony labyrinth, and otoconia were removed using eyelash tool (Ted Pella Inc., cat# 113) under sterile conditions. Dissected utricles were transferred to complete medium that contained DMEM/F12 (Thermo Fisher Scientific, cat# 11320–033), 5% heat-inactivated Fetal Bovine Serum (Thermo Fisher Scientific), and 50U/ml penicillin G (MilliporeSigma). Free floating utricles were cultured overnight in 24- or 48-well culture plates at 37°C and 5% CO_2 prior to any experimental manipulation.

Neomycin sulfate solution (final concentration 3mM, 140mg/ml, VetOne) or cisplatin (final concentration 30μg/ml, WG Critical Care, LLC, Paramus, NJ) was supplemented in complete medium and equilibrated in the incubator for at least 2 h to reestablish a neutral pH. Utricles were then treated with either complete medium or medium supplemented with neomycin or cisplatin and incubated at 37°C and 5% CO_2 for 24 or 45 h. To label apoptotic cells, we incubated utricles in medium containing 7μM CellEvent^{TM} (ThermoFisher Scientific, cat# C10423) that detected activated caspase 3/7 for one hour. Subsequently utricles were fixed for 2–3 h at room temperature in 4% paraformaldehyde (PFA), which was diluted from 16% PFA (Electron Microscopy Sciences, cat# 15710-S) in PBS. The CellEvent^{TM} can only be used in living biological samples, but the fluorescent substrate is stable and retains fluorescence after formaldehyde-based fixation methods.

Immunostaining and confocal image acquisition. Fixed utricles were incubated in blocking buffer (0.3% Triton X-100, 3% NGS, and 2% BSA in PBS) for 1–3 h at room temperature, followed by incubation in primary antibodies (diluted in blocking buffer) overnight at 4°C. The primary antibodies used in this study were directed against myosin 7a (Proteus Bioscience, cat# 25–6790, 1:200), Pou4f3 (Santa Cruz Biotechnology, cat# sc-81980, clone QQ8, 1:200), or oncomodulin (Santa Cruz Biotechnology, cat# sc-7446, 1:200). Utricles were then incubated with Alexa Fluor-conjugated fluorescent secondary antibodies (Thermo Fisher Scientific, 1:500–1:2000 in blocking buffer) for 1 to 2 h at room temperature. Subsequently, utricles are mounted on glass slides using Fluoromount-G aqueous mounting medium (Southern Biotech, cat# 0100–01) and coverslipped to flatten the utricle under the weight of the coverslip. However, due to the three-dimensional bowl-shaped architecture of the utricle, the macula in a whole-mount utricle will not be flat after mounting. Instead, the center of the utricle will be farther away from the coverslip, and the periphery of the macula will be closer to the coverslip. This curvature remains visible under the confocal laser-scanning microscope and increases the number of z-stack images that are required to capture all regions of the macula. Confocal z-stacks with a step size of 0.5 µm will usually generate 25–38 z-stack images that sufficiently capture the entire macula despite the curved surface of the utricle. Additionally, maximum intensity projection accurately represents the z-stack images and only minimally affects the performance of the automated quantification of HCs. However, quantification performed on maximum intensity projection of z-stack images can cause the automated cell counting algorithm to miscount two or more overlapping nuclei as a single nucleus. Therefore, we emphasize the importance of the manual correction step following the automated step.

Z-series images through the entire utricular macula were collected using a x20 0.8 N.A. Plan-Apochromat objective (x0.7 optical zoom) and an Axiovert 200M inverted microscope with a confocal scan head (Carl Zeiss Microscopy LSM780 or LSM880) equipped with an Airyscan detection unit controlled by Zen v2.3 software. Identical settings for pinhole, gain, and offset were used between samples for each experiment. Acquired Airyscan data sets were processed using Zen 2.3 SP1 Black software (Carl Zeiss version 14.0.0.0).

Quantification of HCs. Two methods of HC quantification were performed using the freely available, open-source ImageJ software (Fiji; version 2.1.0; National Institutes of Health, Bethesda, MD). First, we manually quantified myosin 7a-positive HCs from 50 × 50μm (2500μm^2) regions of interest (ROIs) selected from four different regions of each utricle: 5 ROIs in the posterior extrastriola (P-ES), 4 ROIs in the lateral extrastriola (L-ES), 4 ROIs in the medial extrastriola (M-ES), and 4 ROIs in the striola (Fig. 1B). Free statistical computing R software (https://www.r-project.org/) was used to compute all 320 possible combinations of average HC

counts calculated by selecting one ROI from each region within an individual utricle as shown below.

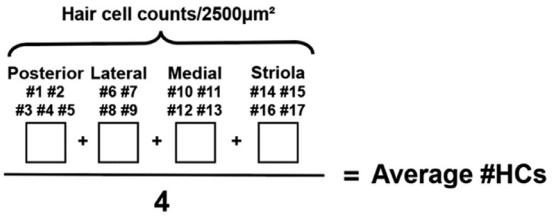

Second, Pou4f3-positive HC nuclei in the entire utricle were quantified both manually and semi-automatically. For semi-automated counts, confocal z-stack images of utricles were imported to ImageJ and merged to generate maximum intensity projection images. The clear separation between the nuclear Pou4f3 fluorescent signal and background allowed for image segmentation using the "Make Binary" command, which automatically calculated the threshold by analyzing the histogram. For lower resolution/quality images, the signal threshold was set manually using the "Threshold" command. Due to the abundance of HCs in control utricles, maximum intensity projection images often contained HC nuclei that appeared to be partially overlapping. To increase the accuracy of the semi-automated quantification, these overlapping nuclei were separated using the "Watershed" command and were counted using the "Analyze Particle" command that generated a numbered outline around each nucleus. The "Analyze Particle" settings (size (micron^2) = 21-infinity and circularity = 0.3–1) were adjusted to reflect the average area of the Pou4f3 signal observed in living HCs, which ranged between 20 and 68 μm^2 (data not shown). These results were added to the "ROI manager" to allow the overlay of the nuclear outlines on the original z-slice image to visually verify HC count accuracy. Finally, a macro was developed to integrate a series of ImageJ commands to simplify the process of automated HC quantification. Examples of the original utricle images, the macro code, and an instructional video are included in the website (https://www.nidcd.nih.gov/research/labs/section-sensory-cell-biology). Following the automated HC count, the original image that was overlayed with the Pou4f3 signal outline was further assessed for mis-quantified HCs and manually corrected using the "Multi-point Tool" to add or subtract HCs in ImageJ to obtain the final HC count. Manual counts were also performed using the "Multi-point Tool" function.

Myosin 7a immunoreactivity and tdTomato expression in utricles from Gfi1-tdTomato mice were used to count HCs using the approach described above. Specifically, tdTomato+ HCs were semi-automatically quantified and myosin 7a+ HCs were manually quantified (myosin 7a-label fills the HC cytoplasm while excluding the nucleus and therefore does not allow for automated counting) from the whole utricle. HC counts from using all three markers were then compared to each other.

The area of the sensory epithelium in control utricles were slightly larger than the area in neomycin-treated utricles in both C57BL/6 and CBA/J mice (Supplemental Fig. 2C). Thus, to standardize the area for our counts, we normalized all the HC counts from the whole utricle to 180,000μm^2, which was determined by averaging the area of the sensory epithelium from control and neomycin-treated utricles.

Quantification of activated caspase 3/7 signal in the sensory epithelium. To quantify dead or dying cells exclusively in the macula of the utricles, activated caspase 3/7 (AC3/7) signal that was detected outside the boundaries of the sensory epithelium or in the stromal layer (where no Pou4f3 labeling is observed) was selectively removed throughout the confocal z-slices using a custom ImageJ macro that is included in the supplementary information. The AC3/7 signal in the sensory epithelium in these images was subsequently quantified using the same macro that was developed to quantify Pou4f3-positive HCs.

Statistics. All statistical analyses were performed using Prism 8 software (GraphPad, San Diego, CA). The Shapiro-Wilks normality test was used to confirm the normal distribution of the data. Student's t-test was used to compare two groups. Comparisons of multiple groups were subjected to ordinary one-way ANOVA with Tukey's post-hoc multiple comparisons test. Data are presented as mean ± SD throughout. Statistical significance is indicated as: (*) $P < 0.05$, (**) $P < 0.01$, (***) $P < 0.001$, (****) $P < 0.0001$. P-value above 0.05 ($P>0.05$) was considered non-significant and is indicated as "ns".

3. Results

3.1. HC numbers vary by region within the utricle

A widely used method to quantify utricular HCs is to manually count myosin 7a-positive HCs in selected ROIs and average the number of HCs per unit area for each utricle (Baker et al., 2015; Burns et al., 2012a; Sayyid et al., 2019; Zhang et al., 2020). To investigate the variability of HC density within the same region of the utricle, HCs in control and neomycin-treated utricles from C57BL/6 WT mice were labeled using myosin 7a and imaged (36x magnification). Five 50 × 50μm (2500μm^2) ROIs were placed in the posterior extrastriolar region (P-ES), and HCs were quantified for each ROI (Fig. 1A). A representative image of a single utricle from the control group showed low variability (6.7%) ranging from 63 to 75 HCs per ROI. In contrast, HC counts from neomycin-treated utricle exhibited higher variability (30.5%) ranging from 19 to 41 HCs per ROI (Fig. 1A). The high variability in neomycin-treated utricle compared to control utricle was verified across multiple utricles (Table 1). Specifically, within neomycin-treated utricles, lower HC counts were consistently observed in ROI #2 (19 HCs) compared to either ROI #1 (41 HCs; $^{**}p = 0.029$) or ROI #5 (37 HCs; $^{*}p = 0.0491$) (Fig. 1A, data not shown). Variability was assessed using coefficient of variation using the formula (HC_{SD}/HC_{mean}) x 100 (Table 1).

Next, we examined whether a regional variation in HC density across the utricle may impact HC counts obtained using the ROI counting method. Control and neomycin-treated utricles from C57BL/6 and CBA/J WT mice were labeled with HC markers myosin 7a, Pou4f3, and the striolar marker oncomodulin. HCs were counted in 4–5 50 × 50μm (2500μm^2) ROIs placed in four utricular regions (P-ES, L-ES, M-ES, and striola) and averaged. Fig. 1B shows placement of these ROIs in a control utricle. In both control and neomycin-treated utricles, the density of HCs was lower in the striolar region than in the ES regions. Interestingly, while the density of HCs was similar in all three ES regions in the control utricles, the M-ES region in the neomycin-treated utricles was more susceptible to neomycin-induced HC death than the P-ES and L-ES regions (Fig. 1C,D), highlighting the variance in HC counts introduced by ROI placement using this method. To investigate the extent to which HC counts vary by ROI selection, we randomly selected one ROI from each of the four regions and averaged the number of HCs for both control and neomycin-treated utricles (Fig. 1E-H). All 320 possible combinations of ROIs per utricle (P-ES: 5 ROIs, L-ES: 4 ROIs, M-ES: 4 ROIs, Striola: 4 ROIs) were used to calculate average HC counts using a free statistical computing software R (https://www.r-project.org/). Depending on the ROI selection within the same utricle, a difference of up to 18 HCs (<5.9% variability) and 13 HCs (<8.3% variability) per 2500μm^2

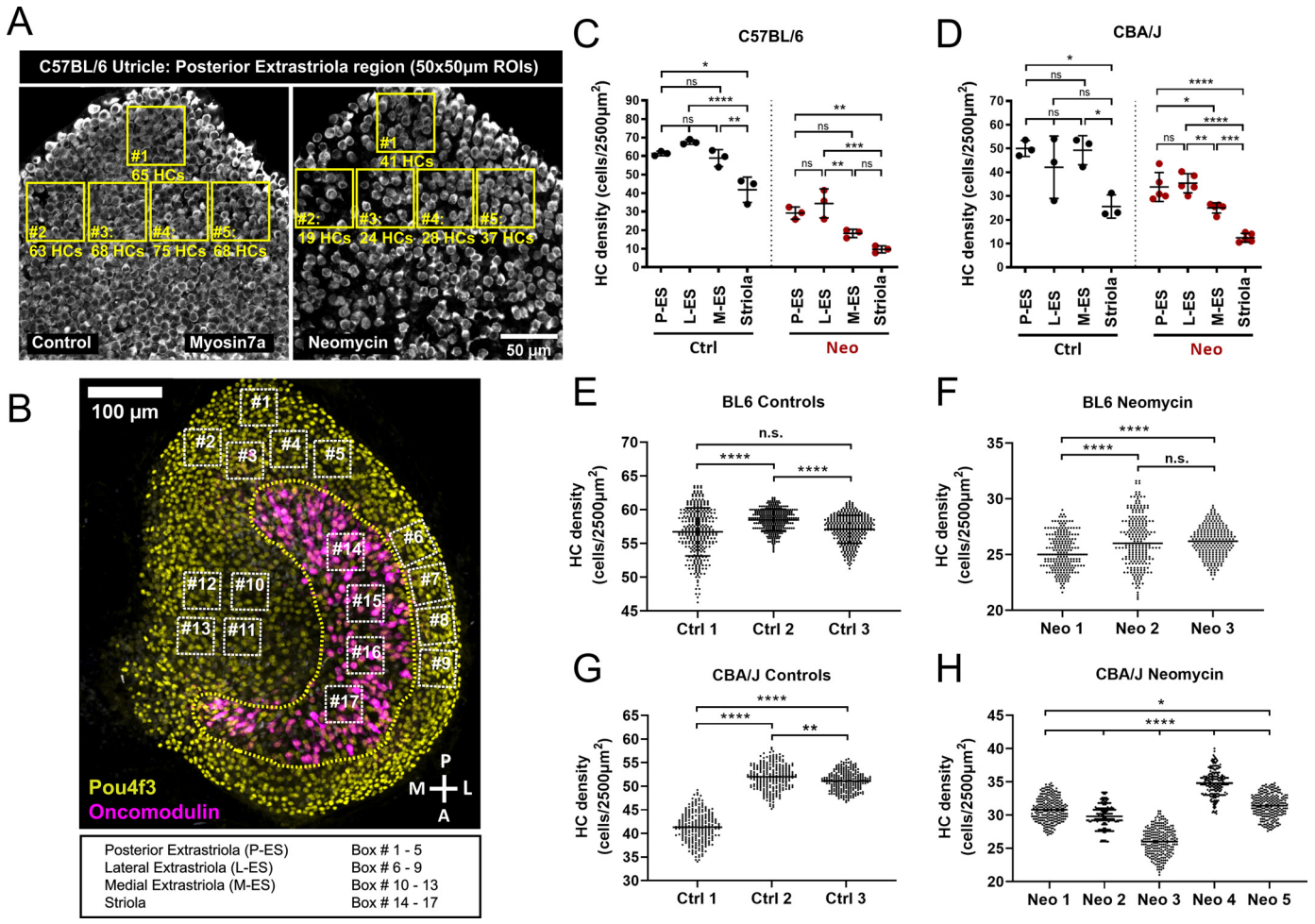

Fig. 1. Regional variation in HC density across the utricle

Utricles were cultured in control or neomycin-containing medium for 24 h and labeled with antibodies against Pou4f3 (yellow), myosin 7a (gray), or oncomodulin (magenta, outlined in yellow dashed line). (A) Five ROIs for HC counting were placed in the P-ES region of both a control and a neomycin-treated utricle. The neomycin-treated utricle demonstrates variable HC densities in the five selected ROIs. Scale bar: 50μm. (B) 4–5 50 × 50μm (2500μm^2) ROIs were placed in four utricular regions (P-ES, L-ES, M-ES, and striola). Scale bar: 100μm. (C,D) HC counts within each ROI were assessed from (C) C57BL/6 and (D) CBA/J WT mice, and the averaged HC density was determined. Each data point represents the average HC density of an individual utricle. In both mouse strains, striolar HC densities are significantly reduced compared to those in the ES in control and neomycin-treated conditions. In addition, HC densities from M-ES are lower than HC densities from other ES regions in the neomycin-treated utricles. (E-H) ROI selection within a region impacts HC quantification. Using one ROI from each of the four regions of the utricle, all 320 possible combinations of ROIs were used to calculate average HC densities from control and neomycin-treated utricles from either (E,F) C57BL/6 or (G,H) CBA/J WT mice. Each data point represents the average HC density of one ROI combination. X-axes labeled in (E-H) indicate individual utricles (Ctrl 1–3 and Neo 1–5). Data indicate the mean ± SD for n = 3–5 utricles per condition. Significance was assessed by one-way ANOVA, followed by Tukey's test to account for multiple comparisons. $^{****}P < 0.0001$, $^{***}P < 0.001$, $^{**}P < 0.01$, $^{*}P < 0.05$, and $P > 0.05$ was denoted as "ns".

Table 1
Variability in HC density per 2500μm^2 ROI.

Postertor ES region: 50×50µm (2500µm^2) ROI #1–5								
			Hair Cell Counts					
Mouse Stain		Treatment	HC_{min}	HC_{max}	Range HC_{max}-HC_{min}	Mean	SD	Coefficient of Variation (HC_{SD}/HC_{mean})×100
C57BL/6	(n=3 urticles from 3 mice)	Control	56	66	10	61	5.38	*8.82*
CBA/J	(n=3 urticles from 3 mice)	Control	48	55	7	50	7.51	15.02
C57BL/6	(n=3 urticles from 3 mice)	Neomycin	23	38	15	29	6.92	23.86
CBA/J	(n=5 urticles from 5 mice)	Neomycin	29	39	10	34	8.21	24.15

HC counts were obtained from five 50 × 50μm (2500μm^2) ROIs placed in the posterior utricular region (P-ES). Average maximum and minimum HC counts from 3 to 5 utricles per group are shown. Standard deviation (SD) was used to derive coefficient of variation using the formula, (HC_{SD}/HC_{mean}) × 100, suggesting that neomycin-treated utricles have higher variability in HC density compared to the control utricles. n values represent the number of utricles.

were observed for control and neomycin-treated utricles respectively (Fig. 1E-H). These data confirm that ROI selection within a region can significantly affect average HC counts, and they emphasize the demand for more accurate and unbiased methods of HC quantification.

3.2. Pou4f3 is a reliable HC nuclear marker suitable for automated HC quantification

To obtain accurate HC counts, we sought to quantify the entire population of HCs from the utricle, thereby avoiding any re-

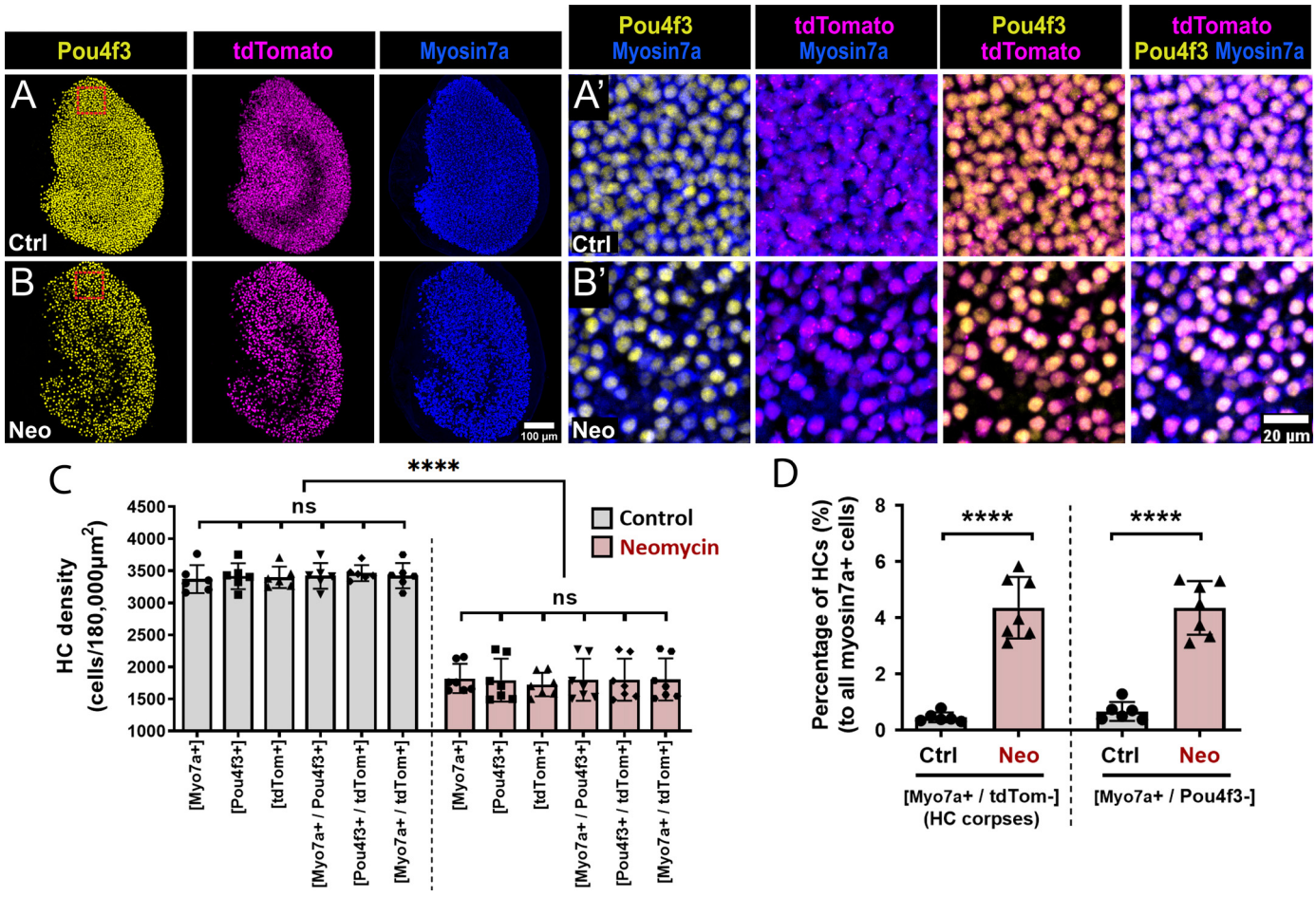

Fig. 2. Pou4f3 is a reliable HC nuclear marker suitable for automated HC quantification
Utricles from Gfi1-tdTomato mice expressing tdTomato in HCs were cultured in either control or neomycin-containing media for 24 h. (A,B) Representative confocal images showing the three HC markers: Pou4f3 (yellow), tdTomato (magenta), and myosin 7a (blue). (A',B') Magnified inset images (from area in the red box in panel A,B) show the posterior region of the utricle. Scale bars: (A,B) 100μm, (A',B') 20μm. (C) HC density obtained using each of the three HC markers resulted in similar HC counts within each group. (D) Compared to controls, neomycin-treated utricles contained significantly more [myosin 7a+/tdTomato-] HC corpses. A similar increase was observed in [myosin 7a+/Pou4f3-] HCs. Data indicate the mean ± SD for n = 6–7 utricles per condition. Significance was assessed by one-way ANOVA, followed by Tukey's test to account for multiple comparisons. $^{****}P < 0.0001$ and $P > 0.05$ was denoted "ns".

gional bias. Previous studies have shown that the number of HCs in freshly dissected and immediately fixed utricles from healthy adult mice ranges from 3200 to 4000 (Burns et al., 2012b; Desai, et al., 2005; Li et al., 2008). Manually counting all utricular HCs, especially in a large data set, is thus a labor-intensive and time-consuming task. Additionally, the commonly used HC marker myosin 7a results in a diffuse cytoplasmic stain that is not conducive to automated quantification and HCs must be counted manually. More importantly, myosin 7a immunolabeling is retained in dead HCs, making it impossible to accurately quantify surviving *vs.* dead HCs after ototoxic drug treatment (Monzack et al., 2015).

Pou4f3 is a HC-specific transcription factor that is present in both developing and mature HCs and is critical for their survival (Erkman et al., 1996; Xiang et al., 1997a). Immunofluorescent staining of Pou4f3 results in a highly specific and discrete nuclear signal in HCs in the adult mouse cochlea and utricle, making it suitable for automated quantification (McInturff et al., 2018; Tong et al., 2015). To identify whether Pou4f3 is a suitable HC marker for automated quantification and labels live HCs, we examined utricles from adult Gfi1$^{Cre/+}$ x B6.Cg-Gt(ROSA)26Sortm14(CAG-tdTomato)Hze/J (Gfi1-tdTomato) mice for tdTomato-positive HCs. This tdTomato label was selected because we have previously demonstrated that, unlike myosin 7a, tdTomato fluorescence is not retained in dead HCs (Monzack et al., 2015). Utricles from these transgenic mice were cultured in control or neomycin-supplemented medium for 24 h, fixed, and labeled with all three HC markers, Pou4f3, tdTomato, and myosin 7a. Single-color and two-color fluorescent images of HC markers showed similar expression patterns and colocalization for all three HC markers (Fig. 2A,A',B,B'). Quantification of HCs using each HC marker individually as well as a combination of two markers showed no statistical differences within each treatment group (Fig. 2C). Meanwhile, we observed a statistically significant reduction in HC counts between control and neomycin groups regardless of which HC markers was used (Fig. 2C). This suggests that all three HC markers resulted in similar HC counts. Using tdTomato as a live cell indicator (Monzack et al., 2015), we found 4-fold increase of [myosin 7a+/tdTomato-] dead HCs (HC corpses) in neomycin-treated utricles compared to controls (Fig. 2D). These data are consistent with our previous report indicating that myosin 7a immunoreactivity is retained in dead HCs. Interestingly, most of these myosin 7a-positive corpses were Pou4f3-negative, suggesting that Pou4f3 immunolabeling is less likely than myosin 7a to be retained in dead HCs in neomycin-treated utricles.

3.3. Pou4f3 and activated caspase 3/7 co-labeling indicates HC viability

To develop a reliable method for confirming HC survival that does not require the use of transgenic mice expressing tdTomato,

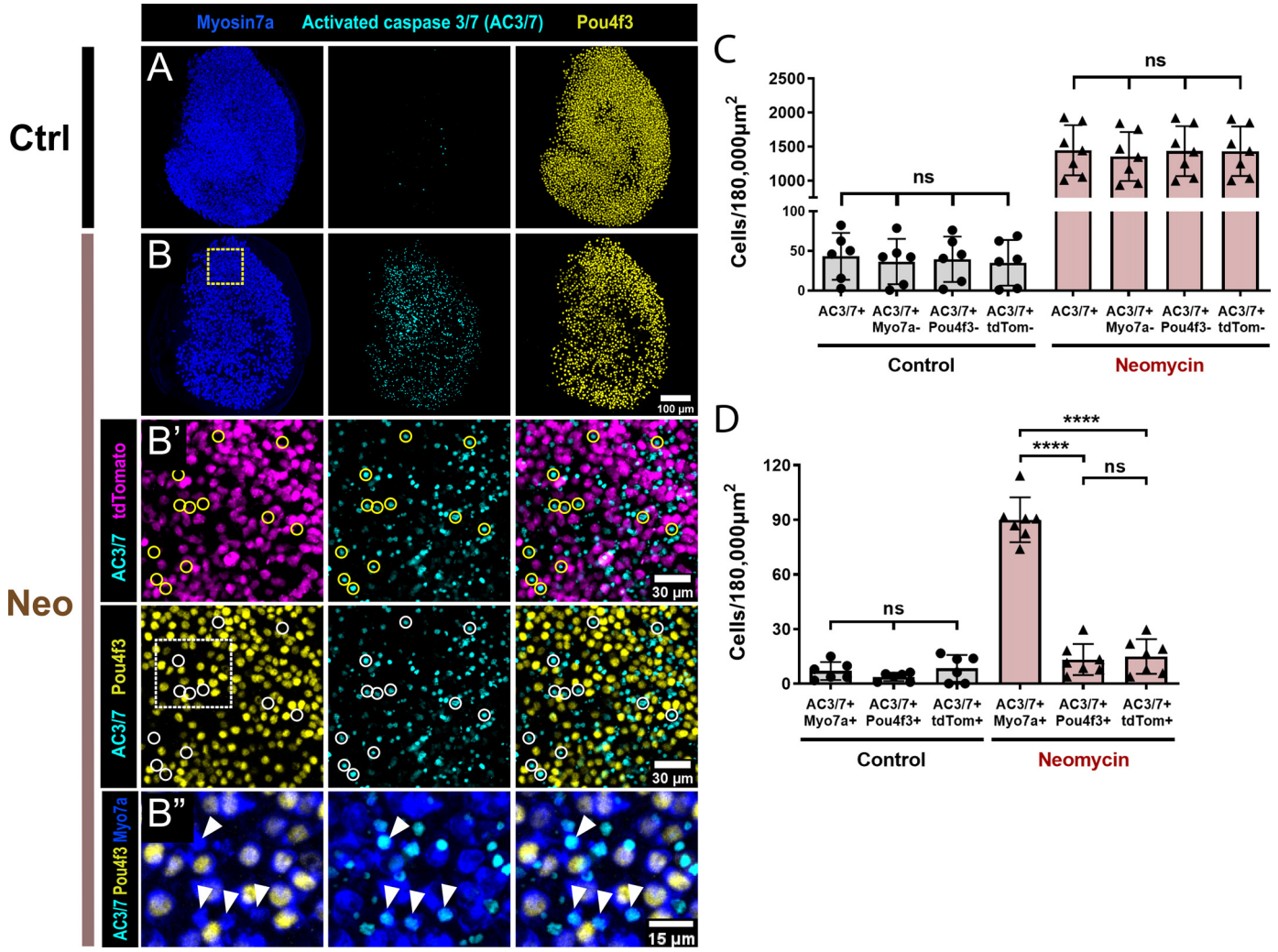

Fig. 3. Pou4f3 and activated caspase 3/7 co-labeling indicate HC viability
CellEvent™ was used to label activated caspase 3/7 (AC3/7) in control and neomycin-treated utricles from Gfi1-tdTomato mice. HC markers, Pou4f3 (yellow), tdTomato (magenta), and myosin 7a (blue), were assessed along with AC3/7 (dead/dying cells; cyan). (A,B) Confocal images of whole-mount utricles show that neomycin results in an increase in AC3/7-positive cells. Scale bar: 100μm. (B') Magnified inset images (from yellow box in panel B) show that AC3/7 expression did not co-localize with either Pou4f3+ cells (white circles) nor tdTomato+ cells (yellow circles) in neomycin-treated utricles. Scale bar: 30μm. (B") Magnified inset images (from white box in panel B') show myosin 7a immunoreactivity in HCs expressing AC3/7. Scale bar: 15μm. (C) Compared to control utricles, neomycin-treated utricles showed a significant increase in HCs expressing AC3/7. (D) In control conditions, ≤0.25% of HCs (43 HCs per 3476 total HCs) expressing AC3/7 retained tdTomato or immunoreactivity for myosin 7a or Pou4f3. In contrast, neomycin-treated tissue shows a significant increase in HCs that express AC3/7 while retaining myosin 7a immunoreactivity (90/1864 HCs, ≤5%). Significantly fewer AC3/7-positive HCs retained Pou4f3 immunoreactivity or tdTomato (14/1803 HCs, ≤0.8%). Data indicate the mean ± SD for n = 6–7 utricles per condition. Significance was assessed by one-way ANOVA, followed by Tukey's test to account for multiple comparisons. $^{****}P < 0.0001$ and $P > 0.05$ was denoted "ns".

we tested the activated caspase 3/7 (AC3/7) marker, CellEvent™, to detect apoptotic cells in the utricle. Control and neomycin-treated utricles from Gfi1-tdTomato expressing mice were labeled for AC3/7. AC3/7 was detected in both the sensory epithelium and the stromal layer of neomycin-treated utricles, suggesting that neomycin killed not only HCs but also cells in the stromal layer. To quantify AC3/7 signals exclusively in the sensory epithelium, an ImageJ macro was generated to remove AC3/7 signal in the stromal layer (Supplemental Fig. 1). Compared to control utricles, neomycin-treated utricles contained significantly more cells expressing AC3/7 (Fig. 3A-C), indicating that AC3/7 efficiently detects dead or dying HCs. On average, only 14 Pou4f3+ or tdTomato+ HCs (<1% of HC population) were positive for AC3/7 per neomycin-treated utricle. This comparison of the AC3/7 signal with tdTomato labeling, a living HC marker (Monzack et al., 2015), verifies that AC3/7 is a reliable marker of HC death. Importantly, both tdTomato and Pou4f3 signal inversely correlated with AC3/7 labeling, suggesting that Pou4f3 labeling correlated with living HCs in the neomycin-treated condition (Fig. 3B'). In contrast, an average of 90 myosin 7a+ HCs (>5% of all myosin 7a+ HCs) were also positive for AC3/7 in the neomycin-treated utricles, again confirming that these were dead HCs that retained myosin 7a immunoreactivity (Fig. 3B",D). Together these data demonstrate that Pou4f3 is a reliable HC nuclear marker that is less likely than myosin 7a to be retained in dead HCs.

3.4. Semi-automated quantification of Pou4f3-positive HC nuclei

Quantification of HC density by counting a subset of HCs in ROIs reduces the accuracy and increases the variability of HC counts due to the intrinsic differences in HC density across different regions of the utricle (Fig. 1). Given that Pou4f3 is a suitable HC marker with a highly specific and discrete nuclear signal, we developed a method for semi-automated quantification of

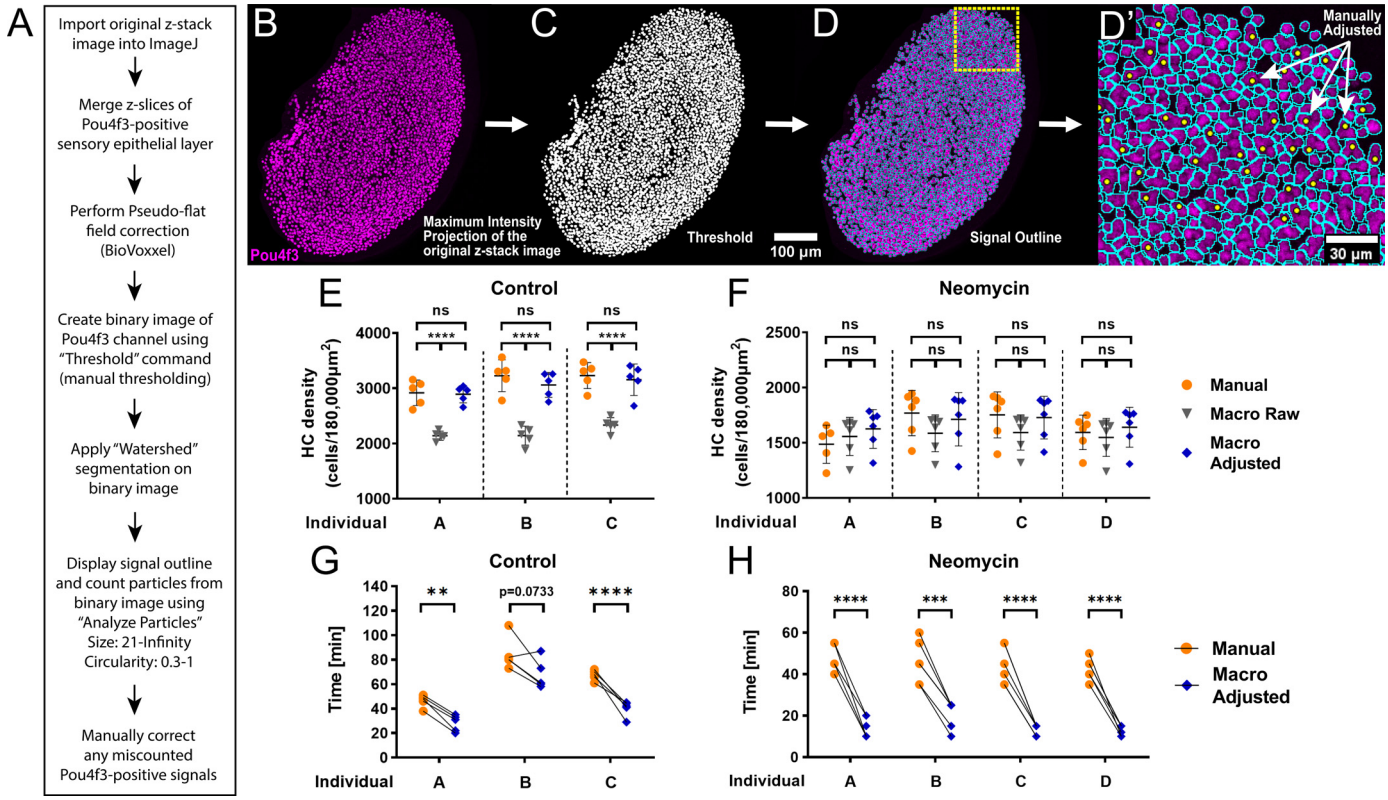

Fig. 4. Semi-automated quantification of Pou4f3-positive HC nuclei using ImageJ macro
(A) Semi-automated analysis algorithm. (B-D,D') Z-stack images of utricles stained for Pou4f3 were acquired using confocal microscopy, imported to ImageJ, and processed using an ImageJ macro that automates Pou4f3-positive (magenta) HC quantification. (B) Pou4f3-positive nuclear signal (magenta) was converted to (C) black and white image (binary image) based on the selected threshold. The "Threshold" function allows the user to choose a cutoff value, determined either manually or automatically by analyzing the histogram of the current image (ImageJ >> Image >> Adjust >> Threshold), in which only pixels above the cutoff value are considered signal. The "Analyze Particles" command measures objects, draws an outline around the signal, and counts the outlined signal in the binary image. The output results can be reviewed via a (D) Pou4f3 signal outline overlay (cyan outline) indicating the counted nuclei, and any mis-quantification can be (D') manually corrected. If more than one Pou4f3 nucleus was present within a single outline after the automated count, the additional Pou4f3 nucleus was manually marked using a yellow dot and added to the overall cell count. Scale bars: (B-D) 100μm (D') 30μm. (E-F) HCs from control and neomycin-treated utricles were quantified by 3–4 observers (Individuals A-D) using both the manual and the semi-automated methods. "Macro Raw" indicates HC counts obtained from the automated method, "Macro Adjusted" indicates the final HC counts following manual correction of HC counts of the automated method (semi-automated method), and "Manual" indicates HCs counted entirely manually using the "Multi-point Tool" function in ImageJ. Significance was assessed by one-way ANOVA, followed by Tukey's test to account for multiple comparisons. (G,H) The semi-automated method significantly reduced the time required to quantify HCs in both (G) control and (H) neomycin-treated utricles. Data indicate the mean ± SD for $n = 6$–7 utricles per condition. Significance between two groups was assessed by unpaired student's t-test. $^{****}P < 0.0001$, $^{***}P < 0.001$, $^{**}P < 0.01$, $^{*}P < 0.05$, and $P > 0.05$ was denoted as "ns".

all the HCs in the entire utricle by staining adult utricles using this marker. To define the nuclear Pou4f3 signal in HCs, images of Pou4f3-stained utricles were processed using the "Threshold" command within ImageJ, a function that allows the users to define both low and high threshold values and only pixels that fall within this specified range are used to generate a binary image. Additionally, the watershed function was utilized to define nuclei borders in areas where nuclei in the maximum intensity projection images were overlapping. The output results were reviewed using the Pou4f3 outline overlay displaying counted HC nuclei, and any mis-quantification was manually corrected (Fig. 4A-D,D'). Lastly, we scripted an ImageJ macro to streamline the entire workflow from raw image loading to the generation of the final quantified image.

To test the accuracy of our semi-automated quantification across users, HCs were counted by 3–4 independent observers (Individuals A-D) using both the manual and the semi-automated methods. While the HC counts using the automated method (Macro Raw; gray upside-down triangle) were initially lower than manual counts (Manual; orange circle) in control conditions, this difference was abolished after users corrected the automated counts using the overlay of Pou4f3 outlines obtained from the automated quantification (Macro Adjusted; blue diamond) (Fig. 4E). In contrast, HC counts from neomycin-treated utricles were not significantly different between manual counts and semi-automated counts for any individual observer (Fig. 4F). Moreover, the semi-automated method significantly reduced the time required to quantify HCs in both control and neomycin-treated utricles. The semi-automated method was on average 21 min faster (time spent reduced by 31%) when counting control utricles and 30.6 min faster (time spent reduced by 66.9%) when counting neomycin-treated utricles (Fig. 4G-H). Together, these data show that the adjusted semi-automated counts were as accurate as manually counting all HCs within an individual utricle, while having the benefit of significantly decreasing the time required to perform the quantification.

3.5. Neither myosin 7a nor Pou4f3 are reliable markers for HC viability in cisplatin-treated utricles

Our previous work demonstrated that SCs actively phagocytose HCs in neomycin-treated utricles, and this phagocytic activity was impaired in cisplatin-treated utricles. This lack of SC-mediated phagocytic activity of dead HCs results in a significantly higher number of [myosin 7a+/tdTomato-] dead HCs (HC corpses) in cisplatin-treated utricles relative to neomycin-treated utricles (Monzack et al., 2015). Given the differences in the cellular re-

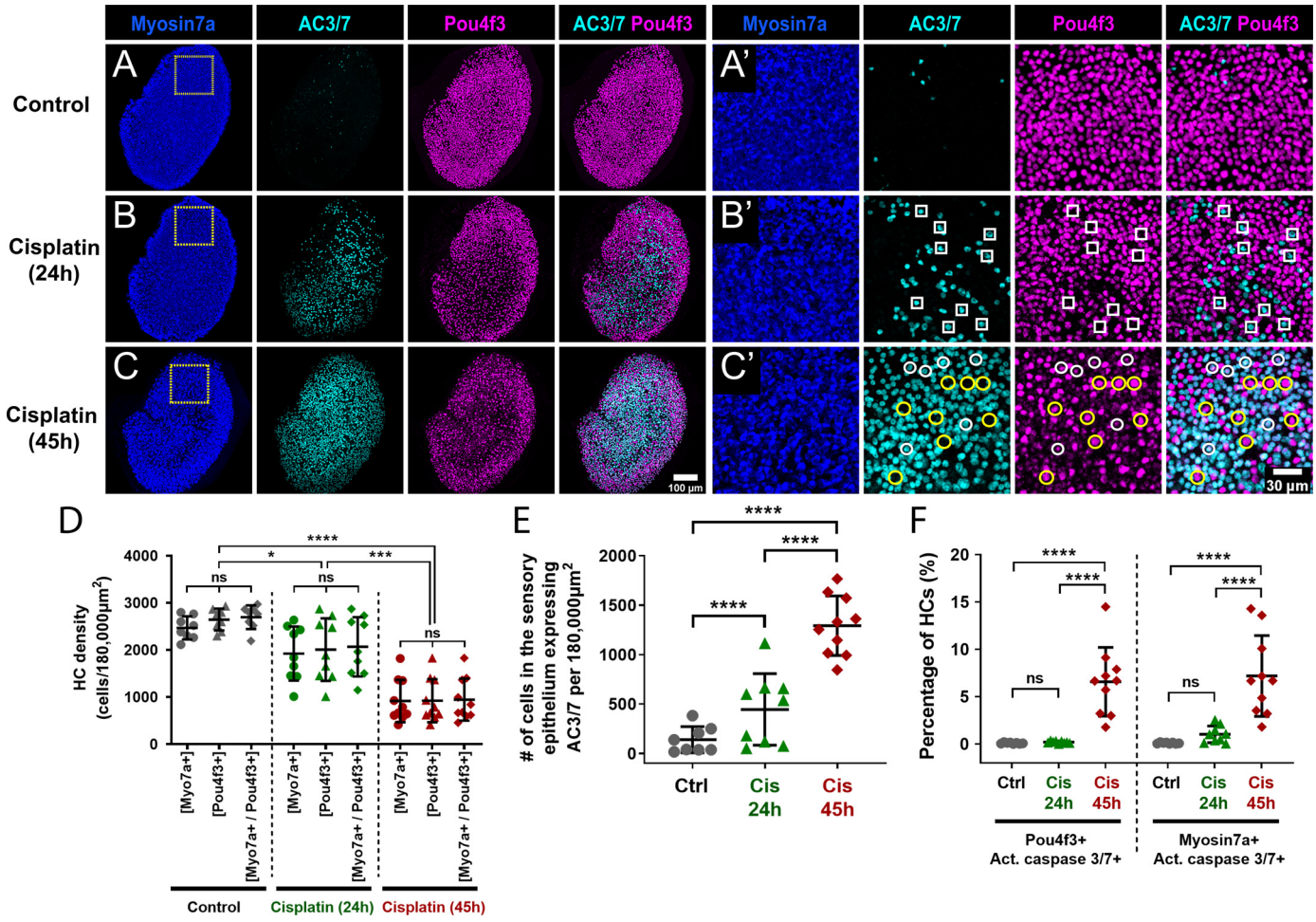

Fig. 5. Cisplatin-treated utricles require a live/dead cell indicator in addition to Pou4f3
Control or cisplatin-treated utricles (24 and 45 h) were labeled for AC3/7, Pou4f3, and myosin 7a. (A-C) Confocal images of cisplatin-treated utricles show increased numbers of cells with AC3/7 at 24 and 45 h compared to control utricles. (A'-C') Magnified inset images (from yellow box in panels A-C). (B') Utricles exposed to cisplatin for 24h exhibited minimal overlap between AC3/7 and Pou4f3 ([AC3/7+/Pou4f3-], white squares). (C') In contrast, utricles exposed to cisplatin for 45 h displayed a significant increase in HCs that showed co-localization of Pou4f3 and AC3/7, indicating that Pou4f3 immunoreactivity is retained in dead HCs at 45 h, ([AC3/7+/Pou4f3+], white circles; [AC3/7-/Pou4f3+], yellow circles). Scale bar: (A-C) 100μm and (A'-C') 30μm. (D) HC density was reduced while (E) AC3/7 expression increased with increasing duration of cisplatin treatment. (F) The percentage of dead/dying HCs (AC3/7-positive) that retain both myosin 7a and Pou4f3 immunoreactivity in cisplatin-treated utricles at 45 h. (D-F) Each data point represents cell counts from an individual utricle. Data indicate the mean ± SD for n = 8–10 utricles per condition. Significance was assessed by one-way ANOVA, followed by Tukey's test to account for multiple comparisons. $^{****}P < 0.0001$, $^{***}P < 0.001$, $^{**}P < 0.01$, $^{*}P < 0.05$, and $P > 0.05$ was denoted "ns".

sponses to these two ototoxic drugs, we tested whether Pou4f3 labeling was co-localized with AC3/7-labeling during cisplatin treatment, contrary to what was observed in neomycin-treated utricles. Control or cisplatin-treated (24 and 45 h) utricles were labeled for AC3/7, Pou4f3, and myosin 7a. Cisplatin-treated utricles showed a significant increase in cells with AC3/7 at both timepoints compared to the control utricles (Figure 5A-C). The number of living HCs [Pou4f3+/AC3/7-] was reduced and AC3/7 expression increased with prolonged duration of cisplatin treatment (Fig. 5D,E). Utricles exposed to cisplatin for 24h exhibited minimal co-expression of AC3/7 and Pou4f3, similar to our observations in neomycin-treated utricles (Fig. 5B'). In contrast, utricles exposed to cisplatin for 45h displayed significant co-expression of AC3/7 and Pou4f3, indicating that Pou4f3 immunoreactivity is retained in dead HCs in cisplatin-treated utricles (Fig. 5C'). A discernable variability in the intensity of the Pou4f3 immunoreactivity suggested that [Pou4f3+/AC3/7-] HCs may display stronger Pou4f3 signal intensity compared to [Pou4f3+/AC3/7+] HCs (Fig. 5C'). However, this difference did not eliminate the need to confirm cell survival and death using a secondary method such as AC3/7 labeling. In addition, similar percentages of Pou4f3-positive and myosin 7a-positive HCs also expressed AC3/7 (Fig. 5F). These results highlight the importance of the use of a secondary method (such as AC3/7 labeling) to confirm HC viability in utricle explants treated with ototoxic drugs, since dead HCs can retain both myosin 7a and Pou4f3 immunoreactivity in cisplatin-treated utricles.

4. Discussion

Whole-organ cultures of utricles from adult mice represent a well-characterized and widely used *ex vivo* preparation for studies of mature mammalian HCs and SCs, particularly in response to ototoxic drugs (Breglio et al., 2020; Burns et al., 2012a; Hartman et al., 2010; Sayyid et al., 2019). Many investigators (ourselves included) who utilize this model system to study the HC responses to ototoxic drugs have visualized HCs by immunostaining cultured utricles for the HC marker myosin 7a. Myosin 7a immunostaining results in cytoplasmic staining that is not conducive to automated cell counting methodologies and must be quantified manually. The standard method to quantify myosin 7a-positive HCs is by placing multiple ROIs in the ES region of each utricle, manually count HCs from each ROI, and calculate the average HC density (Baker et al.,

2015; Burns et al., 2012a; Sayyid et al., 2019; Stone et al., 2018; Zhang et al., 2020). This method assumes that HCs are uniformly distributed throughout the utricle, and that HCs in each ROI are equally susceptible to ototoxic drug-induced HC death. However, in both control and neomycin-treated utricles, the average HC counts per ROI from four regions (P-ES, L-ES, M-ES, and striola) showed variable HC density emphasizing that the specific placement of the ROIs, placed either regionally or broadly across the utricle, can introduce substantial variability in the HC quantification within a single utricle (Fig. 1). Therefore, our results indicate that the most accurate quantification would require counting of all the HCs in the utricle, a time-consuming and labor-intensive task using manual counting methods.

To improve the accuracy and time efficiency of HC quantification, we used the HC-specific transcription factor Pou4f3 to develop a method for automated HC quantification. Pou4f3 is a transcription factor that is selectively expressed in HCs and plays an essential role in their maturation and maintenance in the cochlea and vestibular system (Erkman et al., 1996; McInturff et al., 2018; Tong et al., 2015; Xiang et al., 1997b; Zhang et al., 2016). Importantly, its discrete expression pattern in the nucleus makes Pou4f3 a suitable marker for automated HC quantification.

A number of software applications are available for automated cell quantification including, ImageJ (Schindelin et al., 2012; Schneider et al., 2012), CellProfiler (Carpenter et al., 2006), and Matlab (Mathworks Ltd, Natick, MA). Methods for the quantification of branched microglial cells, apoptotic retinal ganglion cells, or fluorescently labeled migrating cells using a semi-automated cell counting algorithm have been successfully developed in Matlab (Al-Khazraji et al., 2011; Bizrah et al., 2014; de Gracia, et al., 2015; Talebizadeh et al., 2017). However, this commercially available software is expensive and requires computer coding skills. Both CellProfiler and ImageJ are free, open-source image processing packages designed to analyze multidimensional images. In this study, a semi-automated image analysis method was developed in ImageJ to quantify HC nuclei that were labeled with Pou4f3 from the entire utricle. Similar approaches have been used to semi-automatically count a variety of cell features/types, including fluorescently labeled bone marrow-derived macrophage nuclei, dendritic spines, or senescent cells (Lozano-Gerona and Garcia-Otin, 2018; Orlowski and Bjarkam, 2012; Trout and Holian, 2019). Our study is the first to apply this method to counting the HCs from the entire utricle.

While the fully automated approach consistently missed approximately one-third of the total number of HCs in control utricles (2305±107 HCs / 3254±313 total HCs), the semi-automated approach adds a manual correction step following the automated step (approx. 950 HCs). This addition of a manual correction step resulted in HC counts with an accuracy similar to those obtained manually (Fig. 4E). The incomplete detection of HCs in the automated step is primarily attributable to the close proximity of the HC nuclei. When z-stack images of the utricle are projected into a single 2D image, adjacent Pou4f3-positive HC nuclei in different planes may partially overlap, causing the automated cell counting algorithm to miscount two or more overlapping nuclei as a single nucleus. This is in part due to the normal positioning of nuclei of the two types of HCs in the utricle, in which type I HC nuclei are generally located deeper in the sensory epithelium than type II HC nuclei, which are located closer to the luminal surface (Pujol et al., 2014; Sun et al., 2015). This unique three-dimensional anatomical location of HC nuclei poses a challenge to using a fully automated algorithm alone to count HCs. These overlapping nuclei are observed quite frequently in control utricles due to the dense population of HCs. Compared to control utricles, neomycin-treated utricles demonstrated fewer instances of miscounted “overlapping” HCs, with less than 10% error prior to manual adjustment. On average, 1538 HCs were detected by the automated algorithm in neomycin-treated utricles, and 131 HCs were added manually to obtain a total of 1668 HCs. The improved accuracy of the automated cell count in utricles treated with neomycin was likely due to neomycin-induced HC death, which reduced the density of HCs and thus resulted in fewer "overlapping" nuclei. Although our data show no statistical differences between automated (Macro Raw) and semi-automated (Macro Adjusted) HC counts in neomycin-treated utricles (Fig. 4F), we manually check the HC count of every utricle regardless of experimental condition, and we recommend this approach as a mean to maximize accuracy and reproducibility of HC quantification.

The main advantages of the semi-automated method are that it results in accurate counts that are not impacted by regional variation in HC density, and it reduces the time required for HC quantification. Our data indicate that HC quantification using the semi-automated method presented in this study is approximately 21 min faster (time spent reduced by 31%) in control utricles and 30.6 min faster (time spent reduced by 66.9%) in neomycin-treated utricles compared to the manual quantification method (Fig. 4G,H). This is a significant reduction in the time required for quantitative studies, particularly since most studies require several utricles (n = 5–20) in each experimental group (Baker et al., 2015; Breglio et al., 2020; Ku et al., 2014; Li et al., 2008; Wang et al., 2015).

A prerequisite for accurate HC counts using this method of analysis is the requirement to obtain high resolution images of the whole utricle. In this study, we used a Zeiss LSM780 confocal microscope equipped with an Airyscan detector and a 20x/0.8 N.A. lens for the acquisition of high-resolution images. Images of neomycin-treated utricles acquired using traditional confocal microscopy resulted in sufficient resolution to perform semi-automated quantification with high accuracy due to the reduced density of HCs. However, optical resolution required for reliably detecting all HCs in certain utricle regions using the semi-automated method can be at times insufficient in control utricles with dense HC populations. Due to the unique bowl-shaped architecture of the utricle, utricular regions that are farther away from the coverslip will receive more out of focus light, increasing the possibility of spherical aberrations, and reducing the image resolution. Performing semi-automated counts on images acquired under these conditions increases the number of misquantified HCs that users must manually correct. This can be addressed by selecting optimal sampling frequencies, i.e., choosing a sampling interval (the number of pixels and the distance between pixels) equal to twice the highest spatial frequency of the specimen to accurately preserve the spatial resolution in the resulting digital image to achieve the Nyquist criterion, or using an Airyscan detector with improved resolution and signal-to-noise ratio (Huff, 2015).

HCs quantified from the entire utricle can be presented as either “HCs per utricle” or normalized to the area of the macula (e.g. HC density or HC per unit area). Given our observation that the area of the sensory epithelium decreases in neomycin-treated tissue (Supplemental Fig. 2C), presumably due to HC loss, we decided to present HC counts using the latter method. Nonetheless, either choice for presenting utricular HC counts is appropriate and can be used with the semi-automated quantification described herein. Previous reports for total HC numbers from adult animals indicate that utricles from C57BL/6 mice contain more HCs per utricle (3,849±46, P50 and 3,770±106, P80) compared to CBA/J mice (3246±58, adult), consistent with our observation (Burns et al., 2012b; Desai, et al., 2005) (Supplemental Fig. 2A). While the HC counts differed between the two mouse strains, the variability of HC counts was very low (1–3%). Assuming no damage was introduced during utricle dissection, this low variability in the number of HCs across multiple utricles within the same mouse strain sug-

gests that untreated adult utricles contain a consistent HC number. Therefore, when utricles are exposed to ototoxic drugs (e.g. cisplatin or neomycin), the loss of HCs can be solely attributed to the effect of the treatment without any normalization procedures.

However, mouse utricles are small and fragile, and mechanical damage during utricle dissection is a common occurrence. In addition, we have observed that utricles treated with neomycin shrink slightly, leading to variability in the utricle size. The average area of the sensory epithelium in control utricles (C57BL/6 = 194,585±10,234μm^2; CBA/*J* = 186,125±8,229μm^2) are slightly larger than the area in neomycin-treated utricles (C57BL/6 = 183,984±6,995μm^2; CBA/*J* = 176,041±4,167μm^2) (Supplemental Fig. 2C). Therefore, normalization to the macula area can allow the inclusion of utricles with minimal damage incurred during dissection. The average macula area of all utricles, from both control and neomycin treatment groups, used in this study was approximately 180,000μm^2. We used this value to normalize HC counts obtained from the entire utricle. Because 180,000μm^2 is generally smaller than the macula area size of control utricles, the number of HCs can appear lower than what has been reported by others that displayed HC counts per utricle (Burns et al., 2012b; Desai et al., 2005; Golub et al., 2012; Li et al., 2008) (Supplemental Fig. 2A,C). While this normalization can be an effective method to include minimally damaged utricles, it is also important to note that experiments in which the treatment itself can affect the macula area, such as HC regeneration or HC rescue experiments, have the potential to mask the changes in the HC counts when normalized to area size and plotted as HC density. Therefore, when plotting HC counts as density, it is important to confirm that the data agree with data presented as "per utricle".

This semi-automated counting method using the ImageJ macro script can be modified to utilize other tissue biomarkers and is therefore widely applicable for quantifying other subpopulations of cells in the utricle. For example, CellEvent™ is comprised of a non-fluorescent dye conjugated with tetrapeptide sequence Asp-Glu-Val-Asp (DEVD) recognized by caspase 3/7. Activation of caspase 3/7 in apoptotic cells leads to cleavage of the DEVD peptide and the dye translocates to the nucleus where it binds to DNA, resulting in fluorescent signal. Therefore, utricles labeled with CellEvent™ provide a robust nuclear signal that allows quantification of cells undergoing apoptosis using the semi-automated method (Supplemental Fig. 1). In addition, utricles from Gfi1-tdTomato mice express tdTomato in both the cytoplasm and the nucleus of HCs (Monzack et al., 2015), showing discrete tdTomato signal for each HC, making it possible to use the semi-automated method to count tdTomato-positive HCs. Finally, Sox2 is a transcription factor expressed in the nucleus of SCs and type II HCs but not in type I HCs in the utricle (Bucks et al., 2017; Oesterle et al., 2008). The difference in the 3D spatial location, in which type I HC nuclei are located just above the SC nuclei closer to the luminal surface allows easy identification of the two cell types from confocal images of the utricle (Pujol, et al., 2014). Thus, utricular SCs and type II HCs labeled with Sox2 could, in theory, be quantified, respectively, using the semi-automated method presented in this study.

The ability to distinguish between living vs. dead cells is imperative for most studies that utilize HC quantification as an outcome. While Pou4f3 is a well-characterized HC marker, its reliability to detect exclusively living HCs or both living and dead HCs had not been previously examined. We reported that expression of tdTomato in HCs from Atoh1-tdTomato transgenic mice served as a reliable indicator that a HC is alive, while loss of tdTomato expression coincided with loss of membrane integrity and HC death (Monzack et al., 2015). We also reported that the common HC marker myosin 7a is present in both living and dead HCs and cannot be used to indicate HC survival (Monzack et al., 2015). Although Atoh1-tdTomato expression in HCs reliably reports HC viability, it is not practical for all studies to incorporate a transgenic mouse model for this purpose. In this study, we examined whether Pou4f3 immunostaining is retained in dead HCs. Our data indicate that (1) myosin 7a immunoreactivity is retained in dead HCs, consistent with our previous work, and (2) compared to myosin 7a, Pou4f3 immunoreactivity is less likely to be observed in dead HCs in neomycin-treated utricles. However, it is important to note that Pou4f3 immunoreactivity was observed in both live and dead HCs in cisplatin-treated utricles, as discussed below.

In contrast to neomycin treatment, Pou4f3+ HCs corpses were frequently observed in cisplatin-treated utricles (Fig. 5C'). Previous studies have shown that dead HCs are phagocytosed by surrounding SCs to clear cellular debris in both the cochlea and the utricle (Bird et al., 2010; Bucks et al., 2017; Forge et al., 1998; Hayashi et al., 2020; Li et al., 1995; Monzack et al., 2015; Raphael and Altschuler, 1991). Our live-cell imaging studies showed that SCs actively phagocytose HCs that were killed by neomycin treatment, while this phagocytic activity was impaired in cisplatin-treated utricles (Monzack et al., 2015). Our observation of Pou4f3 immunoreactivity in HCs killed by cisplatin exposure is consistent with this model in which cisplatin damages SCs, impairing their ability to engulf and remove dead HCs and resulting in the accumulation of HC corpses in the sensory epithelium.

The duration of myosin 7a or Pou4f3 retention in dead HCs is unknown and determining how long this retention persists will likely require a live imaging approach similar to the one we employed in our previous study (Monzack et al., 2015). Dead HCs are removed by the phagocytic activity of the surrounding SCs (Bird et al., 2010; Monzack et al., 2015). Our previous study suggests that SC phagocytic activity is reduced by nearly 50% in cisplatin-treated utricles compared to neomycin-treated utricles (Monzack et al., 2015). These data are in agreement with our observation that both myosin 7a and Pou4f3 immunoreactivity are retained in dead HCs in cisplatin-treated utricles. Therefore, it is possible that myosin 7a or Pou4f3 may be retained in dead HCs indefinitely until they are engulfed by phagocytes (either SCs or macrophages). Thus, it is critical to use a cell death marker in conjunction with HC markers to identify living HCs. CellEvent™ is limited to treating tissue culture cells or *ex vivo* preparations of organ wholemounts. Therefore, staining with an antibody against cleaved caspase-3 or TUNEL labeling are also appropriate methods for detecting apoptotic cells.

In conclusion, our data indicate that Pou4f3 is a suitable HC nuclear marker for semi-automated HC quantification. However, Pou4f3 immunoreactivity alone does not report whether the labeled HC is alive or dead, particularly in the cisplatin-treated condition, in which dead HCs are not efficiently removed from the sensory epithelium. Thus, for studies in which HC survival is an important outcome measure, it is essential to confirm HC viability using a secondary method, such as AC3/7 labeling. The semi-automated method we present in this study uses an ImageJ macro to quantify Pou4f3-positive HCs in the entire utricle, increasing the accuracy of the quantification of HCs while significantly reducing the time required for accurate quantification. The ImageJ macro code and video providing step by step instructions for using the ImageJ macro cell counter can be found on the website (https://www.nidcd.nih.gov/research/labs/section-sensory-cell-biology).

CRediT authorship contribution statement

Cathy Yea Won Sung: Methodology, Software, Validation, Formal analysis, Investigation, Visualization, Writing – original draft, Writing – review & editing. **Melanie Barzik:** Methodology, Validation, Formal analysis, Investigation, Writing – review & editing. **Tucker Costain:** Methodology, Software, Investigation. **Lizhen**

Wang: Methodology, Software, Formal analysis, Resources, Data curation. **Lisa L. Cunningham:** Writing – review & editing, Supervision, Funding acquisition.

Acknowledgement

This research was supported by the Division of Intramural Research of the NIH, NIDCD (Project no. 1ZIADC000079).

Supplementary materials

Supplementary material associated with this article can be found, in the online version, at doi:10.1016/j.heares.2021.108429.

References

Al-Khazraji, B.K., Medeiros, P.J., Novielli, N.M., Jackson, D.N., 2011. An automated cell-counting algorithm for fluorescently-stained cells in migration assays. Biol. Proced Online 13 (1), 9. doi:10.1186/1480-9222-13-9.

Baker, T.G., Roy, S., Brandon, C.S., Kramarenko, I.K., Francis, S.P., Taleb, M., Marshall, K.M., Schwendener, R., Lee, F.S., Cunningham, L.L., 2015. Heat shock protein-mediated protection against Cisplatin-induced hair cell death. J. Assoc. Res. Otolaryngol. 16 (1), 67–80. doi:10.1007/s10162-014-0491-7.

Bird, J.E., Daudet, N., Warchol, M.E., Gale, J.E., 2010. Supporting cells eliminate dying sensory hair cells to maintain epithelial integrity in the avian inner ear. J. Neurosci. 30 (37), 12545–12556. doi:10.1523/JNEUROSCI.3042-10.2010.

Bizrah, M., Dakin, S.C., Guo, L., Rahman, F., Parnell, M., Normando, E., Nizari, S., Davis, B., Younis, A., Cordeiro, M.F., 2014. A semi-automated technique for labeling and counting of apoptosing retinal cells. BMC Bioinformatics 15, 169. doi:10.1186/1471-2105-15-169.

Brandon, C.S., Voelkel-Johnson, C., May, L.A., Cunningham, L.L., 2012. Dissection of adult mouse utricle and adenovirus-mediated supporting-cell infection. J. Vis. Exp. (61) doi:10.3791/3734.

Breglio, A.M., May, L.A., Barzik, M., Welsh, N.C., Francis, S.P., Costain, T.Q., Wang, L., Anderson, D.E., Petralia, R.S., Wang, Y.X., et al., 2020. Exosomes mediate sensory hair cell protection in the inner ear. J. Clin. Invest. 130 (5), 2657–2672. doi:10.1172/JCI128867.

Bucks, S.A., Cox, B.C., Vlosich, B.A., Manning, J.P., Nguyen, T.B., Stone, J.S., 2017. Supporting cells remove and replace sensory receptor hair cells in a balance organ of adult mice. Elife 6 doi:10.7554/eLife.18128.

Burns, J.C., Cox, B.C., Thiede, B.R., Zuo, J., Corwin, J.T., 2012a. In vivo proliferative regeneration of balance hair cells in newborn mice. J. Neurosci. 32 (19), 6570–6577. doi:10.1523/JNEUROSCI.6274-11.2012.

Burns, J.C., On, D., Baker, W., Collado, M.S., Corwin, J.T., 2012b. Over half the hair cells in the mouse utricle first appear after birth, with significant numbers originating from early postnatal mitotic production in peripheral and striolar growth zones. J. Assoc. Res. Otolaryngol. 13 (5), 609–627. doi:10.1007/s10162-012-0337-0.

Carpenter, A.E., Jones, T.R., Lamprecht, M.R., Clarke, C., Kang, I.H., Friman, O., Guertin, D.A., Chang, J.H., Lindquist, R.A., Moffat, J., et al., 2006. CellProfiler: image analysis software for identifying and quantifying cell phenotypes. Genome Biol. 7 (10), R100. doi:10.1186/gb-2006-7-10-r100.

Coradini, P.P., Cigana, L., Selistre, S.G., Rosito, L.S., Brunetto, A.L., 2007. Ototoxicity from cisplatin therapy in childhood cancer. J. Pediatr. Hematol. Oncol. 29 (6), 355–360. doi:10.1097/MPH.0b013e318059c220.

Cunningham, L.L., 2006. The adult mouse utricle as an in vitro preparation for studies of ototoxic-drug-induced sensory hair cell death. Brain Res. 1091 (1), 277–281. doi:10.1016/j.brainres.2006.01.128.

Cunningham, L.L., Matsui, J.I., Warchol, M.E., Rubel, E.W., 2004. Overexpression of Bcl-2 prevents neomycin-induced hair cell death and caspase-9 activation in the adult mouse utricle in vitro. J. Neurobiol. 60 (1), 89–100. doi:10.1002/neu.20006.

de Gracia, P., Gallego, B.I., Rojas, B., Ramirez, A.I., de Hoz, R., Salazar, J.J., Trivino, A., Ramirez, J.M., 2015. Automatic counting of microglial cells in healthy and glaucomatous mouse retinas. PLoS One 10 (11), e0143278. doi:10.1371/journal.pone.0143278.

Desai, S.S., Zeh, C., Lysakowski, A., 2005. Comparative morphology of rodent vestibular periphery. I. Saccular and utricular maculae. J. Neurophysiol. 93 (1), 251–266. doi:10.1152/jn.00746.2003.

Erkman, L., McEvilly, R.J., Luo, L., Ryan, A.K., Hooshmand, F., O'Connell, S.M., Keithley, E.M., Rapaport, D.H., Ryan, A.F., Rosenfeld, M.G., 1996. Role of transcription factors Brn-3.1 and Brn-3.2 in auditory and visual system development. Nature 381 (6583), 603–606. doi:10.1038/381603a0.

Fausti, S.A., Larson, V.D., Noffsinger, D., Wilson, R.H., Phillips, D.S., Fowler, C.G., 1994. High-frequency audiometric monitoring strategies for early detection of ototoxicity. Ear Hear. 15 (3), 232–239. doi:10.1097/00003446-199406000-00004.

Forge, A., Li, L., Nevill, G., 1998. Hair cell recovery in the vestibular sensory epithelia of mature guinea pigs. J. Comp. Neurol. 397 (1), 69–88.

Golub, J.S., Tong, L., Ngyuen, T.B., Hume, C.R., Palmiter, R.D., Rubel, E.W., Stone, J.S., 2012. Hair cell replacement in adult mouse utricles after targeted ablation of hair cells with diphtheria toxin. J. Neurosci. 32 (43), 15093–15105. doi:10.1523/JNEUROSCI.1709-12.2012.

Hartman, B.H., Reh, T.A., Bermingham-McDonogh, O., 2010. Notch signaling specifies prosensory domains via lateral induction in the developing mammalian inner ear. Proc. Natl. Acad. Sci. U. S. A. 107 (36), 15792–15797. doi:10.1073/pnas.1002827107.

Hayashi, Y., Suzuki, H., Nakajima, W., Uehara, I., Tanimura, A., Himeda, T., Koike, S., Katsuno, T., Kitajiri, S.I., Koyanagi, N., et al., 2020. Cochlear supporting cells function as macrophage-like cells and protect audiosensory receptor hair cells from pathogens. Sci. Rep. 10 (1), 6740. doi:10.1038/s41598-020-63654-9.

Huff, J., 2015. The Airyscan detector from ZEISS: confocal imaging with improved signal-to-noise ratio and super-resolution. Nature Methods 12 (i–ii). doi:10.1038/nmeth.f.388.

Huth, M.E., Ricci, A.J., Cheng, A.G., 2011. Mechanisms of aminoglycoside ototoxicity and targets of hair cell protection. Int. J. Otolaryngol. 2011, 937861. doi:10.1155/2011/937861.

Jen, H.I., Hill, M.C., Tao, L., Sheng, K., Cao, W., Zhang, H., Yu, H.V., Llamas, J., Zong, C., Martin, J.F., et al., 2019. Transcriptomic and epigenetic regulation of hair cell regeneration in the mouse utricle and its potentiation by Atoh1. Elife 8. doi:10.7554/eLife.44328.

Kaur, T., Hirose, K., Rubel, E.W., Warchol, M.E., 2015. Macrophage recruitment and epithelial repair following hair cell injury in the mouse utricle. Front. Cell Neurosci. 9, 150. doi:10.3389/fncel.2015.00150.

Ku, Y.C., Renaud, N.A., Veile, R.A., Helms, C., Voelker, C.C., Warchol, M.E., Lovett, M., 2014. The transcriptome of utricle hair cell regeneration in the avian inner ear. J. Neurosci. 34 (10), 3523–3535. doi:10.1523/JNEUROSCI.2606-13.2014.

Li, A., Xue, J., Peterson, E.H., 2008. Architecture of the mouse utricle: macular organization and hair bundle heights. J. Neurophysiol. 99 (2), 718–733. doi:10.1152/jn.00831.2007.

Li, L., Nevill, G., Forge, A., 1995. Two modes of hair cell loss from the vestibular sensory epithelia of the guinea pig inner ear. J. Comp. Neurol. 355 (3), 405–417. doi:10.1002/cne.903550307.

Lozano-Gerona, J., Garcia-Otin, A.L., 2018. ImageJ-based semiautomatic method to analyze senescence in cell culture. Anal. Biochem. 543, 30–32. doi:10.1016/j.ab.2017.11.020.

Marshak, T., Steiner, M., Kaminer, M., Levy, L., Shupak, A., 2014. Prevention of cisplatin-induced hearing loss by intratympanic dexamethasone: a randomized controlled study. Otolaryngol. Head Neck Surg. 150 (6), 983–990. doi:10.1177/0194599814524894.

Matern, M., Vijayakumar, S., Margulies, Z., Milon, B., Song, Y., Elkon, R., Zhang, X., Jones, S.M., Hertzano, R., 2017. Gfi1(Cre) mice have early onset progressive hearing loss and induce recombination in numerous inner ear non-hair cells. Sci. Rep. 7, 42079. doi:10.1038/srep42079.

McInturff, S., Burns, J.C., Kelley, M.W., 2018. Characterization of spatial and temporal development of Type I and Type II hair cells in the mouse utricle using new cell-type-specific markers. Biol. Open 7 (11). doi:10.1242/bio.038083.

Monzack, E.L., May, L.A., Roy, S., Gale, J.E., Cunningham, L.L., 2015. Live imaging the phagocytic activity of inner ear supporting cells in response to hair cell death. Cell Death Differ. 22 (12), 1995–2005. doi:10.1038/cdd.2015.48.

Oesterle, E.C., Campbell, S., Taylor, R.R., Forge, A., Hume, C.R., 2008. Sox2 and JAGGED1 expression in normal and drug-damaged adult mouse inner ear. J. Assoc. Res. Otolaryngol. 9 (1), 65–89. doi:10.1007/s10162-007-0106-7.

Ono, K., Keller, J., Lopez Ramirez, O., Gonzalez Garrido, A., Zobeiri, O.A., Chang, H.H.V., Vijayakumar, S., Ayiotis, A., Duester, G., Della Santina, C.C., et al., 2020. Retinoic acid degradation shapes zonal development of vestibular organs and sensitivity to transient linear accelerations. Nat. Commun. 11 (1), 63. doi:10.1038/s41467-019-13710-4.

Orlowski, D., Bjarkam, C.R., 2012. A simple reproducible and time saving method of semi-automatic dendrite spine density estimation compared to manual spine counting. J. Neurosci. Methods 208 (2), 128–133. doi:10.1016/j.jneumeth.2012.05.009.

Petersen, T., Rogers, C., 2015. Aminoglycoside-induced hearing deficits – a review of cochlear ototoxicity. South African Family Practice 57 (2). doi:10.1080/20786190.2014.1002220.

Pujol, R., Pickett, S.B., Nguyen, T.B., Stone, J.S., 2014. Large basolateral processes on type II hair cells are novel processing units in mammalian vestibular organs. J. Comp. Neurol. 522 (14), 3141–3159. doi:10.1002/cne.23625.

Raphael, Y., Altschuler, R.A., 1991. Scar formation after drug-induced cochlear insult. Hear. Res. 51 (2), 173–183. doi:10.1016/0378-5955(91)90034-7.

Sadler, E., Ryals, M.M., May, L.A., Martin, D., Welsh, N., Boger, E.T., Morell, R.J., Hertzano, R., Cunningham, L.L., 2020. Cell-specific transcriptional responses to heat shock in the mouse utricle epithelium. Front. Cell Neurosci. 14, 123. doi:10.3389/fncel.2020.00123.

Sayyid, Z.N., Wang, T., Chen, L., Jones, S.M., Cheng, A.G., 2019. Atoh1 Directs Regeneration and Functional Recovery of the Mature Mouse Vestibular System. Cell Rep. 28 (2), 312–324. doi:10.1016/j.celrep.2019.06.028, e314.

Schindelin, J., Arganda-Carreras, I., Frise, E., Kaynig, V., Longair, M., Pietzsch, T., Preibisch, S., Rueden, C., Saalfeld, S., Schmid, B., et al., 2012. Fiji: an open-source platform for biological-image analysis. Nat. Methods 9 (7), 676–682. doi:10.1038/nmeth.2019.

Schneider, C.A., Rasband, W.S., Eliceiri, K.W., 2012. NIH Image to ImageJ: 25 years of image analysis. Nat. Methods 9 (7), 671–675. doi:10.1038/nmeth.2089.

Stone, J.S., Wisner, S.R., Bucks, S.A., Mellado Lagarde, M.M., Cox, B.C., 2018. Characterization of adult vestibular organs in 11 CreER Mouse Lines. J. Assoc. Res. Otolaryngol. 19 (4), 381–399. doi:10.1007/s10162-018-0676-6.

Sun, D.Q., Lehar, M., Dai, C., Swarthout, L., Lauer, A.M., Carey, J.P., Mitchell, D.E., Cullen, K.E., Della Santina, C.C., 2015. Histopathologic changes of the inner ear in rhesus monkeys after intratympanic gentamicin injection and vestibular pros-

thesis electrode array implantation. J. Assoc. Res. Otolaryngol. 16 (3), 373–387. doi:10.1007/s10162-015-0515-y.
Talebizadeh, N., Hagstrom, N.Z., Yu, Z., Kronschlager, M., Soderberg, P., Wahlby, C., 2017. Objective automated quantification of fluorescence signal in histological sections of rat lens. Cytometry A 91 (8), 815–821. doi:10.1002/cyto.a.23131.
Tong, L., Strong, M.K., Kaur, T., Juiz, J.M., Oesterle, E.C., Hume, C., Warchol, M.E., Palmiter, R.D., Rubel, E.W., 2015. Selective deletion of cochlear hair cells causes rapid age-dependent changes in spiral ganglion and cochlear nucleus neurons. J. Neurosci. 35 (20), 7878–7891. doi:10.1523/JNEUROSCI.2179-14.2015.
Trout, K.L., Holian, A., 2019. Factors influencing multinucleated giant cell formation in vitro. Immunobiology 224 (6), 834–842. doi:10.1016/j.imbio.2019.08.002.
Wang, T., Chai, R., Kim, G.S., Pham, N., Jansson, L., Nguyen, D.H., Kuo, B., May, L.A., Zuo, J., Cunningham, L.L., et al., 2015. Lgr5+ cells regenerate hair cells via proliferation and direct transdifferentiation in damaged neonatal mouse utricle. Nat. Commun. 6, 6613. doi:10.1038/ncomms7613.
Woodson, E., 2013. Sensorineural hearing loss (ototoxicity). In: Kountakis, S.E. (Ed.), Encyclopedia of Otolaryngology, Head and Neck Surgery. Springer, Berlin, Heidelberg doi:10.1007/978-3-642-23499-6.
Xiang, M., Gan, L., Li, D., Chen, Z.Y., Zhou, L., O'Malley Jr., B.W., Klein, W., Nathans, J., 1997a. Essential role of POU-domain factor Brn-3c in auditory and vestibular hair cell development. Proc. Natl. Acad. Sci. U. S. A. 94 (17), 9445–9450. doi:10.1073/pnas.94.17.9445.
Xiang, M., Gan, L., Li, D., Zhou, L., Chen, Z.Y., Wagner, D., O'Malley Jr., B.W., Klein, W., Nathans, J., 1997b. Role of the Brn-3 family of POU-domain genes in the development of the auditory/vestibular, somatosensory, and visual systems. Cold Spring Harb. Symp. Quant. Biol. 62, 325–336.
Zhang, C., Wang, M., Xiao, Y., Zhang, F., Zhou, Y., Li, J., Zheng, Q., Bai, X., Wang, H., 2016. A Novel Nonsense Mutation of POU4F3 Gene Causes Autosomal Dominant Hearing Loss. Neural Plast. 2016, 1512831. doi:10.1155/2016/1512831.
Zhang, Y., Zhang, S., Zhang, Z., Dong, Y., Ma, X., Qiang, R., Chen, Y., Gao, X., Zhao, C., Chen, F., et al., 2020. Knockdown of Foxg1 in Sox9+ supporting cells increases the trans-differentiation of supporting cells into hair cells in the neonatal mouse utricle. Aging (Albany NY) 12 (20), 19834–19851. doi:10.18632/aging.104009.